



HAL
open science

Yb:YAG single-crystal fiber amplifiers for picosecond lasers using divided pulse amplification technique

Fabien Lesparre, Jean Thomas Gomes, Xavier Delen, Igor Martial, Julien Didierjean, Wolfgang Pallmann, Bojan Resan, Frédéric Druon, François Balembois, Patrick Georges

► To cite this version:

Fabien Lesparre, Jean Thomas Gomes, Xavier Delen, Igor Martial, Julien Didierjean, et al.. Yb:YAG single-crystal fiber amplifiers for picosecond lasers using divided pulse amplification technique. Photonics West 2016, LASE, Solid State Lasers XXV: Technology and Devices, Feb 2016, San Francisco, United States. hal-01581957

HAL Id: hal-01581957

<https://iogs.hal.science/hal-01581957v1>

Submitted on 14 Sep 2022

HAL is a multi-disciplinary open access archive for the deposit and dissemination of scientific research documents, whether they are published or not. The documents may come from teaching and research institutions in France or abroad, or from public or private research centers.

L'archive ouverte pluridisciplinaire **HAL**, est destinée au dépôt et à la diffusion de documents scientifiques de niveau recherche, publiés ou non, émanant des établissements d'enseignement et de recherche français ou étrangers, des laboratoires publics ou privés.



Distributed under a Creative Commons Attribution - NonCommercial 4.0 International License

Yb:YAG single-crystal fiber amplifiers for picosecond lasers using the divided pulse amplification technique

FABIEN LESPARRE,^{1,2,*} JEAN THOMAS GOMES,¹ XAVIER DÉLEN,¹ IGOR MARTIAL,² JULIEN DIDIERJEAN,² WOLFGANG PALLMANN,³ BOJAN RESAN,³ FREDERIC DRUON,¹ FRANÇOIS BALEMBOIS,¹ AND PATRICK GEORGES¹

¹Laboratoire Charles Fabry, Institut d'Optique Graduate School, CNRS, Université Paris-Saclay, 91127 Palaiseau cedex, France

²FiberCryst SAS, Parc d'activité Wilson Bât A1, 31 Rue Wilson, F-69150 Decines Charpieu, France

³Lumentum, Ruetistrasse 12, 8952 Schlieren, Switzerland

*Corresponding author: fabien.lesparre@institutoptique.fr

A two-stage master-oscillator power-amplifier (MOPA) system based on Yb:YAG single-crystal-fiber (SCF) technology and designed for high peak power is studied to significantly increase the pulse energy of a low-power picosecond laser. The first SCF amplifier has been designed for high gain. Using a gain medium optimized in terms of doping concentration and length, an optical gain of 32 dB has been demonstrated. The second amplifier stage designed for high energy using the divided pulse technique allows us to generate a recombined output pulse energy of 2 mJ at 12.5 kHz with a pulse duration of 6 ps corresponding to a peak power of 320 MW. Average powers ranging from 25 to 55 W with repetition rates varying from 12.5 to 500 kHz have been demonstrated.

OCIS codes: (140.3615) Lasers, ytterbium; (140.3538) Lasers, pulsed; (140.3280) Laser amplifiers; (060.3510) Lasers, fiber.

The requirements of industrial and scientific applications have driven a lot of research and development work on high-power ultrafast diode-pumped solid-state laser systems. In the last few years, among technologies such as fiber, slab, or thin disk, the single-crystal fiber (SCF) has demonstrated strong potential for the development of laser systems with simple and compact geometries. In the continuous wave regime, 250 W was generated from a SCF-based oscillator [1], showing the strong potential of this concept for high power extraction. More recently, SCF amplifiers for short pulses with high-gain and high-nonlinearity thresholds have been demonstrated. In the femtosecond regime, high-repetition-rate systems based on SCF allow high average power, 160 W in linear polarization [2], and 85 W in cylindrical polarization [3]. In the high-energy regime, a common way to push the limit of low-repetition-rate systems using SCF, bulk crystals, or fibers is to exploit the large spectral width of femtosecond pulses to decrease the nonlinear

effects by stretching the input pulses and recompressing the amplified pulses. This way, a SCF amplifier has generated 400 femtosecond pulses with an energy higher than 1 mJ [4]. Recent experimental efforts to improve the performance of high-energy ultrafast sources have focused on coherent combining. The idea is to create several independently amplified pulses, in the space or time domain, in order to decrease the peak intensity in the gain medium. By combining the chirped pulse amplification (CPA) technique and the spatial distribution of the amplification process onto two SCF channels, compressed pulses with durations of 695 fs and energies of 3 mJ were recently obtained [5]. The divided pulse amplification (DPA) concept is an alternative passive coherent combining technique [6,7,8] which has been successfully implemented in femtosecond-fiber-CPA systems to generate pulse energies of 1 mJ [9]. It consists of the generation of pulse replicas with birefringent crystals or delay lines and recombines them after amplification. It can be easily implemented passively in double-pass amplifiers using a 90° polarization rotation between the two passes. In the picosecond regime, the narrow spectral width does not allow easy and efficient exploitation of the CPA technique and DPA is therefore an attractive alternative. Recent studies have demonstrated the possibility of amplifying picosecond pulses in SCF without relying on CPA for pulse energies beyond 700 μJ and peak powers of 28 MW [10]. Implementing DPA on SCF amplifiers opens the way to high-energy direct picosecond pulse amplification with peak powers over 100 MW.

In this Letter, we present a high-energy picosecond laser system based on a low-power picosecond mode-locked oscillator amplified in a two-stage SCF amplifier. In the picosecond regime, due to the low spectral width, in our case below 1 nm, CPA techniques are less convenient to implement compared to the femtosecond regime [4]. For simplicity, the strategy employed here to push further the limitations in terms of peak power and energy is only based on DPA. The combination of a high-gain amplifier stage and a high-energy amplifier stage

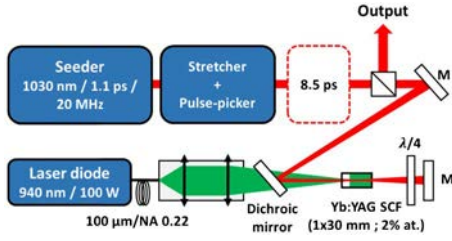


Fig. 1. Experimental setup of the high-gain amplifier stage.

using DPA allows us to demonstrate an average power of 55 W at 500 kHz and a pulse energy of 2 mJ at 12.5 kHz with a pulse duration below 6 ps corresponding to a peak power of 320 MW.

The experimental setup of the first SCF amplifier stage is shown in Fig. 1. The Yb:YAG oscillator delivers a train of pulses of 1.1 ps at 20 MHz with a spectral width of 1.08 nm FWHM centered at a wavelength 1030 nm. A stretcher based on the Martinez design inducing a negative chirp is used to increase the pulse duration to 8.5 ps and reduce the nonlinear effects that occur mainly in the second stage. The alternative option to the stretcher could have been to generate more replicas with the DPA system described later in this article. Using an external pulse picker, the repetition rate can be adjusted between 2 MHz and 12.5 kHz, corresponding respectively to an available average power ranging from 78 mW to 400 μW. The first Yb:YAG SCF amplifier is operated in a double-pass configuration. A dichroic mirror which transmits the pump beam is used to reflect the signal into the SCF. The double pass of the beam is realized by a quarter-wave plate placed after the SCF in order to obtain a 90° rotation of the polarization between the first and the second pass. The polarizer separates the output from the input beam after the second pass. The SCF is a water-cooled Taranis module. The pump and signal beam waists are located about 4 mm after the entrance face of the SCF and have a diameter of 400 μm at the beam waist. Our optical design maximizes pump power on both stages. Experimentally, the pump power defines the position of the return mirror for the second pass in order to adapt the beam parameters to the thermal lens.

This first amplifier stage is designed for high gain, where the key parameter is the overlap between pump and signal beams. In this regard, the SCF is pumped by a high-brightness laser diode delivering 100 W at a wavelength of 940 nm through a fiber with a core diameter of 100 μm and a NA of 0.22. The pump and signal beam waists both have a diameter of 400 μm and are located about 4 mm after the entrance face of the SCF. Since the spatial overlap is potentially the strongest in the first millimeters of propagation in the SCF, it is crucial to maximize the population inversion rate in this region. In order to increase the pump absorption in the entrance of the SCF, the ytterbium doping ratio is pushed to 2% at. Furthermore, by shortening the SCF length to 30 mm, the reabsorption at the signal wavelength is limited, leading to higher optical gains.

The amplified output power obtained in the double-pass configuration at the maximum pump power is shown in Fig. 2(a) for a repetition rate fixed at 2 MHz. A remarkable optical gain of 32 dB is obtained in the small signal regime by injecting 240 μW in this first amplifier stage. To determine the maximum percentage of the amplified spontaneous emission

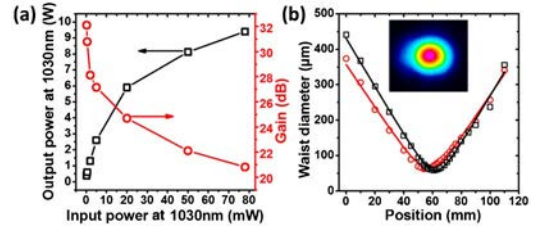


Fig. 2. (a) Output average power (black) and amplification gain (red) versus input power. (b) Beam caustic along the transverse orthogonal axis at maximum output power. Inset: far-field beam profile.

(ASE) in the output power, we measure the amplifier output power at full pump power without a signal. Using this method, the ASE is estimated to be less than 2.5%. A maximum output power of 9.4 W is extracted from the SCF for a seed average power of 78 mW, corresponding to a gain of 21 dB. The energy and peak power of the amplified pulses are respectively 17 μJ and 1.8 MW. The output beam M^2 is below 1.2 in both directions, close to the oscillator, showing that there is no significant degradation [Fig. 2(b)].

The second SCF amplifier also operates in the double-pass configuration, as presented in Fig. 3. The pump and signal have a diameter of 400 μm at the beam waist. The setup is very similar to the first amplifier stage, but this time the SCF is pumped at 969 nm using a wavelength-stabilized laser diode delivering 185 W. Pumping into the zero-phonon transition at 969 nm theoretically reduces the thermal load by 30% as compared to pumping at 940 nm while preserving the absorption efficiency in the SCF [3]. To distribute the thermal load along the SCF and maintain the beam quality during amplification, the doping concentration is also reduced to 1%.

Designed for high pulse energy, the DPA technique is implemented on the second amplification stage. To prevent self-focusing limitations, the peak power of the input pulses is artificially decreased by creating several temporal replicas before amplification. The output replicas are recombined in a totally passive method by polarization switching between the input and output paths; this way, the pulses travel exactly the same optical path length during the round trip. A free-space delay line (FSDL) is first used to generate the two first replicas separated by 300 ps. Then, with a 40 mm long YVO₄ AR-coated crystal, two other replicas temporally separated by 32 ps are generated. The use of a free-delay line allows us to limit the number of YVO₄ crystals and, consequently, the nonlinearities in the recombination phase. By introducing decreasing delays, we generate temporal replicas alternatively linearly and

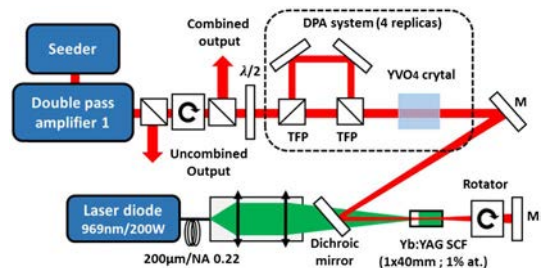


Fig. 3. Experimental setup of the high-energy divided pulse amplifier stage. TFP, thin film polarizer.

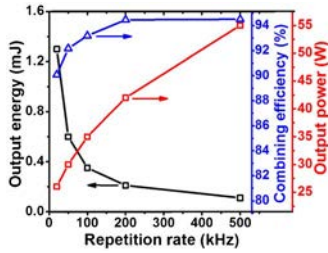


Fig. 4. Output pulse energy (black), output power (red) of the combined pulses, and combining efficiency (blue) versus repetition rate.

orthogonally polarized in the time domain. The theoretical reachable combining efficiencies are thus less limited by interaction effects between replicas. Experimentally, the combining efficiency is defined as follows:

$$\eta = \frac{P_{\text{combined}}}{P_{\text{combined}} + P_{\text{uncombined}}},$$

where P_{combined} and $P_{\text{uncombined}}$ correspond, respectively, to the average power combined and uncombined. The uncombined energy at full pump power is lost as cross polarization from the last output polarizer and then stopped by the isolator toward the pre-amp and seeder.

We first investigate the energy extraction capability by reducing progressively the repetition rate from 500 to 20 kHz. At full pump power, pulse energies of 110 μJ at 500 kHz and 1.3 mJ at 20 kHz are obtained after double-pass amplification (Fig. 4). The peak power of the recombined pulses reaches, respectively, 18 and 208 MW at 500 and 20 kHz.

By increasing the energy level, the coherent combining efficiency slightly decreases from 95% to 90%. The measurement of the temporal combining efficiency has been done using a photodiode and an autocorrelator. Indeed, because of the two different time scales of the delay lines, it is not possible to use only one measurement for both. The amount of energy contained in the satellite pulses is estimated to be less than 0.5% compared to the main pulse. Considering this observation, we focused our work on a careful measurement of the output peak power.

At the lowest repetition of 20 kHz, the peak power per replica reaches 52 MW at the end of the amplification. As the critical peak power of YAG is 1.3 MW, we could expect self-focusing inducing a decrease of the beam size on the output facet of the SCF. To analyze this effect, the beam on the output facet is monitored while increasing the input power at constant repetition rate. As shown in Fig. 5(a), the beam profiles observed after amplification show only very slight degradations, more associated with the increase of the thermal loads by increasing the input power than to self-focusing itself. At maximum output peak power, the B-integral accumulated by the amplified pulses after two passes in the SCF reaches only 2 rad. At this level, the first effects of SPM on negatively chirp pulses can be observed in the spectrum. They are manifested by a slight spectral narrowing and the onset of side lobes, as shown in Fig. 5(b), which is in good agreement with the peak power involved as shown with our simulations. As shown in Fig. 5(c), at constant output peak power per replica, the B-integral accumulated during the amplification decreases in a logarithmic manner with the gain increase. By ensuring an amplification

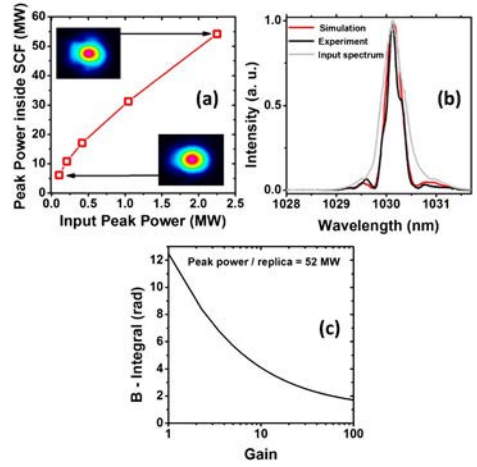


Fig. 5. (a) Output peak power per pulse versus input peak power per pulse. Inset: beam profiles of the output facet of the SCF at low and high peak powers. (b) Experimental (black) and simulated (red) output spectrum at maximum output peak power. (c) B-integral accumulated along the double-pass amplification versus gain amplification at a constant output peak power per pulse of 52 MW.

gain typically higher than 50, the length of YAG experienced at high peak power is reduced and the B-integral accumulated during the amplification does not exceed 2 rad for output peak power per pulse beyond 52 MW. In this case, the main part of the nonlinear effects is clearly located at the end of the amplification medium. We note that while our power amplifier operates well above the critical power for self-focusing, no damage is incurred since the beam size is large enough that the self-focusing critical length exceeds the length of the gain crystal [11].

We finally tried to push further the limits in pulse energy. Using the acousto-optic modulator pulse picker, we decrease the repetition rate down to 12.5 kHz. After being amplified in the first high-gain amplifier stage, the average power is 400 mW, already corresponding to a peak power of 5 MW. To operate in a safe configuration and maintain a low level of nonlinearities during the amplification, the number of replicas is pushed to 8 using a free-space delay line and two YVO_4 crystals of 40 and 20 mm in length. The input peak power is thus divided by a factor 8, falling to 625 kW per replica. The combined and uncombined powers are plotted in Fig. 6(a). At maximum pump power, the amplification gain is above 60 and the output power reaches 25 W, corresponding to an energy of 2 mJ. Despite the peak power of 41 MW per replica, the B-integral accumulated after the double-pass amplification does not exceed 1.6 rad. The maximum combining efficiency decreases from 98% to 86% as the output energy increases. The second stage operates in a saturated amplification regime compare to the first one operating in small signal regime. As a consequence, the amount of ASE produced in the second stage is estimated to be less than 3% even if the pump power is twice higher (200 W).

The limitations of combination efficiency in passive DPA have been discussed in Ref. [12] for the case of fiber amplifiers. We stress that in our bulk crystal amplifier, gain saturation effects play a smaller role compared to fibers. In fact, we estimate that gain saturation can account for about 2% degradation in combination efficiency. Therefore, other effects must also contribute in our case. Experimentally, the slight efficiency drop at

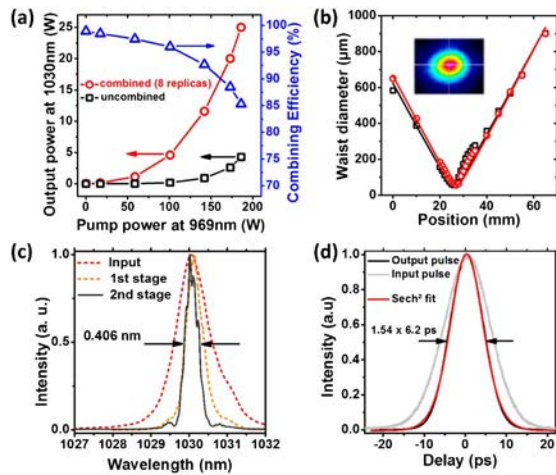


Fig. 6. (a) Combined (red) and uncombined (black) output powers and combining efficiency (blue) versus pump power at 969 nm. (b) Combined beam caustic along two transverse orthogonal axes for the output pulse energy of 2 mJ. Inset: far-field beam profile. (c) Input and output spectra after each amplification stage. (d) Autocorrelation traces of the input and output pulses.

high energies could be explained by an imperfect balance of the energy distribution between replicas during the division process. To maintain the highest possible combining efficiency, a careful adjustment of the half-wave plates, placed before the FSDL and the YVO_4 , that controls the amount of energy sent into each time-domain replica is necessary. At low levels of nonlinearities, the effects of an imperfect balance of energy distribution between replicas on the combining efficiency is almost invisible. It is thus possible to obtain experimentally combining efficiencies higher than 95% without difficulty. As nonlinearities increased, the compensation of the differential phase by adjusting the half-wave plates is more and more critical, which could explain the drop in combining efficiency in the high-peak-power regime. One way to retrieve higher combining efficiencies would be to generate other replicas and thus decrease the peak power in the amplifier. However, we have limited the complexity of our setup to a maximum of 8 replicas.

As shown in Fig. 6(b), the output beam characterization reveals good beam quality with a M^2 below 1.1 in both directions, even at high energy (typically 2 mJ). The autocorrelation trace of the recombined output pulses is plotted in Fig. 6(d). At maximum pulse energy, the pulse duration is 6.2 ps, assuming a sech^2 temporal shape. This leads to a peak power of 320 MW. The spectral width is reduced by gain narrowing from 1 to 0.4 nm [Fig. 6(c)]. It is to be noted that the spectral narrowing

also leads to a temporal narrowing due to the spectrally chirped seed pulses.

In conclusion, we demonstrate that the implementation of a straightforward 2-stage-SCF MOPA chain using the divided pulse process can lead to the generation of pulse energies in the millijoule range from the narrow spectrum (typically around 1 nm) picosecond oscillator. By associating a high-gain amplifier stage generating optical gains up to 32 dB and a divided pulse amplifier able to support high peak powers, pulse energies up to 2 mJ have been obtained. Midway between the fibers and the bulk, SCF provides high gains adapted to very low input powers until a few hundreds of microwatts while preserving a low ASE level in the kilohertz regime and a high tolerance for high peak power of a few tens of megawatts. High output peak powers per replica of up to 50 MW are demonstrated while preserving a low level of nonlinearities during the amplification (B-integral under 2 rad). As a consequence, with a relatively low number of replicas (up to 8) generated with DPA, picosecond pulses with peak powers above 320 MW have been generated after recombination. Finally, repetition rate flexibility between 12.5 and 500 kHz has been demonstrated with average power ranging from 25 to 55 W.

Funding. European Union Seventh Framework Programme (FP7/20072013) (619237).

REFERENCES

1. X. Délen, S. Piehler, J. Didierjean, N. Aubry, A. Voss, M. A. Ahmed, T. Graf, F. Balembos, and P. Georges, *Opt. Lett.* **37**, 2898 (2012).
2. V. Markovic, A. Rohrbacher, P. Hofmann, W. Pallmann, S. Pierrot, and B. Resan, *Opt. Express* **23**, 25883 (2015).
3. F. Lesparre, J.-T. Gomes, X. Délen, I. Martial, J. Didierjean, W. Pallmann, B. Resan, M. Eckerle, T. Graf, M. Abdou Ahmed, F. Druon, F. Balembos, and P. Georges, *Opt. Lett.* **40**, 2517 (2015).
4. X. Délen, Y. Zaouter, I. Martial, N. Aubry, J. Didierjean, C. Hönninger, E. Mottay, F. Balembos, and P. Georges, *Opt. Lett.* **38**, 109 (2013).
5. M. Kienel, M. Müller, S. Demmler, J. Rothhardt, A. Klenke, T. Eidam, J. Limpert, and A. Tünnermann, *Opt. Lett.* **39**, 3278 (2014).
6. Y. Zaouter, F. Guichard, L. Daniault, M. Hanna, F. Morin, C. Hönninger, E. Mottay, F. Druon, and P. Georges, *Opt. Lett.* **38**, 106 (2013).
7. L. J. Kong, L. M. Zhao, S. Lefrancois, D. G. Ouzounov, C. X. Yang, and F. W. Wise, *Opt. Lett.* **37**, 253 (2012).
8. S. Zhou, F. W. Wise, and D. G. Ouzounov, *Opt. Lett.* **32**, 871 (2007).
9. F. Guichard, Y. Zaouter, M. Hanna, K.-L. Mai, F. Morin, C. Hönninger, E. Mottay, and P. Georges, *Opt. Lett.* **40**, 89 (2015).
10. J. Saby, D. Sangla, P. Deslandes, and F. Salin, *Advanced Solid State Lasers*, OSA Technical Digest (online) (Optical Society of America, 2014), paper ATh2A.28.
11. J. Pouysegur, F. Guichard, Y. Zaouter, M. Hanna, F. Druon, C. Hönninger, E. Mottay, and P. Georges, *Opt. Lett.* **40**, 5184 (2015).
12. M. Kienel, A. Klenke, T. Eidam, M. Baumgartl, C. Jauregui, J. Limpert, and A. Tünnermann, *Opt. Express* **21**, 29031 (2013).